High-Resolution Epitope Positioning of a Large Collection of Neutralizing and Nonneutralizing Single-Domain Antibodies on the Enzymatic and Binding Subunits of Ricin Toxin

AMERICAN SOCIETY FOR MICROBIOLOGY | Clinical and Vaccine Immunology®

CLINICAL IMMUNOLOGY

High-Resolution Epitope Positioning of a Large Collection of Neutralizing and Nonneutralizing Single-Domain Antibodies on the Enzymatic and Binding Subunits of Ricin Toxin

David J. Vance,[a] Jacqueline M. Tremblay,[b] Yinghui Rong,[a] Siva Krishna Angalakurthi,[c] David B. Volkin,[c] C. Russell Middaugh,[c] David D. Weis,[d] Charles B. Shoemaker,[b] Nicholas J. Mantis[a,e]

Division of Infectious Disease, Wadsworth Center, New York State Department of Health, Albany, New York, USA[a]; Department of Infectious Disease and Global Health, Tufts Cummings School of Veterinary Medicine, North Grafton, Massachusetts, USA[b]; Department of Pharmaceutical Chemistry, Macromolecule and Vaccine Stabilization Center, University of Kansas, Lawrence, Kansas, USA[c]; Department of Chemistry, University of Kansas, Lawrence, Kansas, USA[d]; Department of Biomedical Sciences, University at Albany, SUNY, Albany, New York, USA[e]

ABSTRACT We previously produced a heavy-chain-only antibody (Ab) VH domain (V_HH)-displayed phage library from two alpacas that had been immunized with ricin toxoid and nontoxic mixtures of the enzymatic ricin toxin A subunit (RTA) and binding ricin toxin B subunit (RTB) (D. J. Vance, J. M. Tremblay, N. J. Mantis, and C. B. Shoemaker, J Biol Chem 288:36538–36547, 2013, https://doi.org/10.1074/jbc.M113.519207). Initial and subsequent screens of that library by direct enzyme-linked immunosorbent assay (ELISA) yielded more than two dozen unique RTA- and RTB-specific V_HHs, including 10 whose structures were subsequently solved in complex with RTA. To generate a more complete antigenic map of ricin toxin and to define the epitopes associated with toxin-neutralizing activity, we subjected the V_HH-displayed phage library to additional "pannings" on both receptor-bound ricin and antibody-captured ricin. We now report the full-length DNA sequences, binding affinities, and neutralizing activities of 68 unique V_HHs: 31 against RTA, 33 against RTB, and 4 against ricin holotoxin. Epitope positioning was achieved through cross-competition ELISAs performed with a panel of monoclonal antibodies (MAbs) and verified, in some instances, with hydrogen-deuterium exchange mass spectrometry. The 68 V_HHs grouped into more than 20 different competition bins. The RTA-specific V_HHs with strong toxin-neutralizing activities were confined to bins that overlapped two previously identified neutralizing hot spots, termed clusters I and II. The four RTB-specific V_HHs with potent toxin-neutralizing activity grouped within three adjacent bins situated at the RTA-RTB interface near cluster II. These results provide important insights into epitope interrelationships on the surface of ricin and delineate regions of vulnerability that can be exploited for the purpose of vaccine and therapeutic development.

KEYWORDS antibody, biodefense, epitope, neutralizing, toxins, vaccines

Ricin is the prototype of the type II ribosome-inactivating protein (RIP) family of toxins (1). Ricin toxin A subunit (RTA) is an RNA N-glycosidase that catalyzes the hydrolysis of a conserved adenine residue within the sarcin/ricin loop (SRL) of 28S rRNA, resulting in ribosome arrest and apoptosis (2–4). Ricin toxin B subunit (RTB) is a galactose- and N-acetylgalactosamine (Gal/GalNAc)-specific lectin that promotes toxin entry into mammalian cells, including the epithelial cells that line the respiratory tract

Received 8 August 2017 **Returned for modification** 2 September 2017 **Accepted** 2 October 2017

Accepted manuscript posted online 11 October 2017

Citation Vance DJ, Tremblay JM, Rong Y, Angalakurthi SK, Volkin DB, Middaugh CR, Weis DD, Shoemaker CB, Mantis NJ. 2017. High-resolution epitope positioning of a large collection of neutralizing and nonneutralizing single-domain antibodies on the enzymatic and binding subunits of ricin toxin. Clin Vaccine Immunol 24:e00236-17. https://doi.org/10.1128/CVI.00236-17.

Editor Marcela F. Pasetti, University of Maryland School of Medicine

Address correspondence to David J. Vance, david.vance@health.ny.gov, or Nicholas J. Mantis, nicholas.mantis@health.ny.gov.

For a companion article on this topic, see https://doi.org/10.1128/CVI.00237-17.

For a commentary on this article, see https://doi.org/10.1128/CVI.00275-17.

(5, 6). Following endocytosis, RTB mediates the retrograde transport of ricin to the *trans*-Golgi network (TGN) and endoplasmic reticulum (ER). Once within the ER, the disulfide bond that links RTA to RTB is reduced by protein disulfide isomerase and RTA is retrotranslocated (dislocated) into the cell cytoplasm, where it triggers programmed cell death (7, 8). Ricin is classified as a category B biothreat agent by the Centers for Disease Control and Prevention (CDC) because of its potential, when delivered via aerosol, to induce severe lung inflammation and tissue damage (9, 10). Concerns over ricin's possible use as a biothreat agent stem from the fact that the toxin is relatively easy to procure from its natural source, castor beans (*Ricinus communis*), as well as from its extreme toxicity following inhalation or injection (11).

As part of a longstanding effort to engineer ricin antitoxins and immunotherapies, we previously produced a library of phage-displayed, heavy-chain-only antibodies (Abs; V_HHs) from two alpacas that had been hyperimmunized with nontoxic mixtures of recombinant RTA, RTB, and ricin toxoid; the library is referred to here as "HobJo" in reference to the names of the two immunized alpacas, Hobbs and Johnnes (12). In our initial study, the phage-displayed V_HH library was subjected to high- and low-stringency "panning" on purified native RTA or RTB that had been immobilized on plastic substrates. This initial screening strategy yielded 11 unique RTA-specific V_HHs and 9 unique RTB-specific V_HHs. Five (4 RTA-specific and 1 RTB-specific) V_HHs among the original 20 had strong or moderate *in vitro* toxin-neutralizing activity (TNA), while the remaining 15 had weak TNA or no detectable TNA. A collection of homo- and heterodimeric (i.e., bispecific) V_HHs were engineered with these original 20 V_HHs and shown to have enhanced avidities for ricin and, in some cases, the capacity to passively protect mice from lethal-dose ricin challenge (12–15). As discussed below, the X-ray crystal structures of 10 different V_HH-RTA complexes, including 7 V_HHs from the original screen (16–18), have been solved to date.

The original strategy of panning the V_HH library onto RTA- and RTB-coated immunotubes presented several drawbacks. First, there was a bias for V_HHs directed against a single immunodominant region on RTA that we refer to as cluster I. Cluster I is defined by the murine monoclonal antibody (MAb) PB10, which recognizes a linear epitope encompassing α-helix B (residues 94 to 107) of RTA (see Fig. S1 in the supplemental material) (19–21). α-Helix B is a secondary motif conserved across the RIP family (22). Approximately half of the original RTA-specific V_HHs recognized epitopes in cluster I, based on competition enzyme-linked immunosorbent assays (ELISAs) performed with PB10. The second shortcoming associated with the original screen was that it gave rise to V_HHs that recognized cryptic epitopes that are exposed when RTA and RTB are adsorbed to polystyrene but that are not accessible to antibodies when ricin is in its native conformation. Finally, by performing screening with individual subunits, rather than with the holotoxin, we were likely missing antibodies directed against quaternary epitopes. With the long-term goal of generating a saturating B cell epitope map of ricin toxin using the HobJo library, which is estimated to contain $\sim 4 \times 10^6$ independent clones, we reasoned that it would be necessary to derive novel panning strategies.

To generate a more complete antigenic map of ricin toxin and to better define the epitopes associated with neutralizing activity, we have now subjected the HobJo V_HH-displayed phage library to pannings on both receptor-bound and antibody-captured ricin holotoxins or subunits. We identified a total of 68 unique ricin-specific V_HHs (31 against RTA, 33 against RTB, and 4 against ricin holotoxin) and present their full-length DNA sequences, binding affinities, and neutralizing activities. We used cross-competition ELISAs with a panel of well-characterized murine monoclonal antibodies (MAbs) as a strategy to localize the epitopes recognized by the new collection of V_HHs. Epitope positioning was validated with available X-ray crystal structures and, in some instances, was followed up with hydrogen-deuterium mass spectrometry (HX-MS). We identified more than 20 different competition bins (a bin was comprised of all V_HHs which shared the same competition profile) that cover >50% of RTA's surface area and an indefinite amount of RTB. Having this comprehensive collection of well-characterized, ricin-specific V_HHs provides important insights into epitope interre-

TABLE 1 Summary of HobJo screens

Screen[c]	Target(s)[d]	No. of V_HHs with indicated specificity[a]				TNA[b]			
		A	B	R	Total	+++	++	+	−
1	RTA	11	0	0	11	2	2	2	5
2	RTB	0	9	0	9	1	0	0	8
3	RTA	7	0	0	7	0	2	2	3
4	RTB	0	9	0	9	0	0	0	9
5	R-ASF	5	0	1	6	0	1	1	4
6	R-PB10	5	2	0	7	1	0	1	5
7	Peptides	0	0	0	0	0	0	0	0
8	RTB-ASF	0	5	0	5	0	0	1	4
9	R-F5 + F6	4[e]	8	3	15[e]	3	2	0	9
Total		31	33	4	68[e]	7	7	7	47

[a]A, RTA; B, RTB; R, ricin holotoxin.
[b]Toxin neutralizing activity, based on IC_{50}, indicated as follows: +++, $IC_{50} < 10$ nM; ++, $IC_{50} < 100$ nM; +, $IC_{50} < 500$ nM; −, $IC_{50} > 500$ nM or undetectable.
[c]V_HHs in screens 1 and 2 were reported previously (12).
[d]R-ASF, ricin captured by ASF; R-PB10, ricin captured by PB10; RTB-ASF, RTB captured by ASF; R-F5 + F6, ricin captured with V_HH JIV-F5 and then blocked with excess JIV-F6.
[e]One anti-RTA V_HH from screen 9 was not successfully expressed and thus was not characterized for TNA and also was not included in the final V_HH total of 68.

lationships on the surface of ricin and delineates two or possibly three regions of vulnerability that can be exploited for the purpose of vaccine and therapeutic development.

RESULTS

In an effort to obtain a comprehensive map of toxin-neutralizing and nonneutralizing B cell epitopes on the surface of ricin, the HobJo V_HH phage display library was subjected to nine different screens (Table 1). Screens 1 to 4 involved panning on immunotubes coated with RTA or RTB and yielded a total of 36 ricin-specific V_HHs (Tables 1 and 2). The 20 V_HHs resulting from screens 1 and 2 were described previously and included 11 against RTA (6 with TNA) and 9 against RTB (1 with TNA) (12). We successfully solved the X-ray crystal structures of seven of those V_HHs in complex with RTA (16–18). Screens 3 and 4 yielded an additional 16 ricin-specific V_HHs, including 7 against RTA, 1 of which was successfully crystallized (17), and 9 against RTB (Table 1).

Screens 5 and 6 were designed to circumvent two issues that we had encountered in screens 1 to 4. First, roughly half of the 36 V_HHs from screens 1 to 4 failed to bind soluble ricin (R), even though they recognized plate-adsorbed ricin (R′), RTA (A′), or RTB (B′). This finding is consistent with the exposure of cryptic epitopes on protein antigens under conditions of binding to polystyrene surfaces (23, 24). Second, the majority of the RTA-specific V_HHs were directed against cluster I, which is defined functionally by competition with MAb PB10 and is known to be immunodominant (12). To overcome these issues, the HobJo library was panned, in screen 5, on ricin captured with asialofetuin (R-ASF) to approximate the conformation of soluble ricin and, in screen 6, on ricin that was captured with PB10 (R-PB10) to mask immunodominant epitopes within cluster I. V_HHs identified in screen 5 were cross-checked for binding to R-PB10, while V_HHs identified in screen 6 were cross-checked for reactivity with R-ASF. Only V_HHs that were positive in both assays were characterized further (Tables 1 and 2). This strategy yielded a total of 56 V_HHs that were reactive with both R-ASF and R-PB10. After we eliminated siblings from the pool, a total of 13 V_HHs remained: 10 against RTA, 2 against RTB, and 1 specific for ricin holotoxin.

Screen 7 was designed to identify V_HHs that recognize two different linear epitopes on RTA defined by the murine toxin-neutralizing MAbs PB10 and SyH7 (19). Two biotin-tagged 18-mer peptides, E12 and G3, corresponding to the core epitopes of PB10 and SyH7, respectively, were captured on immunotubes via the use of avidin and then subjected to panning with the HobJo library. The screen proved unsuccessful,

TABLE 2 Properties of ricin-specific V_HHs described in this study

V_HH	Screen[a]	GenBank accession no.	PDB ID[b]	TNA[c]	K_D (nM)[d]	Specificity[e]	Cluster(s)[f]	Family[g]
JIV-F5	1	KF746018	4Z9K	+++	0.019	A	I	
JIV-F6	1	KF746019		−	1.86	A	III	JIV-F6
JIV-G12	1	KF746020	4LGS	+	0.129	A	I	
JIY-A7	1	KF746021	4LHQ	−	4.3	A	I	JIY-A7
JIY-D9	1	KF746022		−	0.174	A	I + II	JIY-D9
JIY-D10	1	KF746023	4LGR	++	0.114	A	I + II	
JIY-E1	1	KF746024	5BOZ	+	0.686	A	II	
JIY-E3	1	KF746025		−	0.296	A	I	
JIY-E5	1	KF746026	4LGP	+++	0.191	A	I + IV	
JIY-F10	1	KF746027		−	NB	A′		
JIY-G11	1	KF746028	4LHJ	++	0.553	A	I	
JIW-B1	2	KF746029		−	NB	B′		
JIW-C12	2	KF746030		−	NB	B′		
JIW-D12	2	KF746031		−	NB	B′		JIZ-B7
JIW-G5	2	KF746032		−	NB	B′		
JIW-G10	2	KF746033		−	NB	B′		JIW-G10
JIZ-B7	2	KF746034		+++	0.031	B	SII	JIZ-B7
JIZ-B9	2	KF746035		−	NB	B′		
JIZ-D8	2	KF746036		−	NB	B′		
JIZ-G4	2	KF746037		−	NB	B′		
JNM-A11	3	KY824576		−	0.200	A	I	
JNM-B5	3	KY824577		−	0.060	A	I	
JNM-C12	3	KY824578		++	0.099	A	I + IV	
JNM-D1	3	KY824579		−	1.19	A	II + III	
JNM-E4	3	KY824580		++	0.083	A	I	
JNM-F8	3	KY824581	5E1H	+	0.203	A	I	
JNM-G4	3	KY824582		+	0.128	A	I	JIY-A7
JNN-A3	4	KY824583		−	NB	B′		JIW-G10
JNN-B6	4	KY824584		−	NB	B′		
JNN-B8	4	KY824585		−	NB	B′		JIZ-B7
JNN-C5	4	KY824586		−	NB	B′		
JNN-C8	4	KY824587		−	NB	B′		
JNN-D1	4	KY824588		−	NB	B′		JIZ-B7
JNN-D8	4	KY824589		−	NB	B′		
JNN-E4	4	KY824590		−	NB	B′		
JNN-H9	4	KY824591		−	NB	B′		
V1B4	5	KY824592		−	4.09	R	SII	
V1B10	5	KY824593		+	0.917	A	III	JIV-F6
V1B11	5	KY824594		−	8.84	A	I + III	
V1C7	5	KY824595	5J56	−	3.19	A	II	V1C7
V1D3	5	KY824596		++	0.460	A	III	JIV-F6
V1G6	5	KY824597		−	5.34	A	III	V2G10
V2A11	6	KY824598		−	1.82	A	III	
V2B8	6	KY824599		−	32.4	A	I + II	JIY-D9
V2B9	6	KY824600		−	1.03	A	II	V1C7
V2C11	6	KY824601		+++	0.015	B	SII	V2C11
V2D4	6	KY824602		+	3.2	B	SII	V2C11
V2E8	6	KY824603		−	5.74	A	II	V1C7
V2G10	6	KY824604		−	1.16	A	III	V2G10
V4A1	8	KY824605		+	0.667	B	SII	
V4C6	8	KY824606		−	NB	B		V4C6
V4C8	8	KY824607		−	NB	B		V4C6
V4D12	8	KY824608		−	NB	B		
V4G3	8	KY824609		−	NB	B		
V5A2	9	KY824610		−	1.46	A	III	
V5B1	9	KY824611		−	2.17	B		
V5B6	9	KY824612		−	0.668	B		
V5C1	9	KY824613		++	0.301	A	II	V1C7
V5C4	9	KY824614		−	5.01	B		
V5D1	9	KY824615		++	0.216	R	SII	
V5D5	9	KY824616		−	5.54	B		
V5E1	9	KY824617	5J57	+++	0.019	A	II	
V5E4	9	KY824618		+++	0.006	B	SII	
V5G1	9	KY824619		+++	0.106	B	SII	

(Continued on next page)

TABLE 2 (Continued)

V_HH	Screen[a]	GenBank accession no.	PDB ID[b]	TNA[c]	K_D (nM)[d]	Specificity[e]	Cluster(s)[f]	Family[g]
V5G6	9	KY824620		−	1.24	R	SII	
V5G12	9	KY824621		−	0.994	R	SII	
V5H2	9	KY824622		−	2.18	B	SII	V2C11
V5H6	9	KY824623		−	23.2	B		

[a]V_HHs in screens 1 and 2 were reported previously (12).
[b]Protein Data Bank IDs.
[c]Toxin-neutralizing activity (TNA), as described in the legend of Table 1.
[d]NB, no binding detected in SPR.
[e]A, RTA; A′, RTA′; B, RTB; B′, RTB′; R, ricin holotoxin.
[f]Data represent RTA epitope cluster(s) (I to IV) bound by a particular V_HH. SII refers to "supercluster II" and is the designation given to RTB- or holotoxin-specific V_HHs that are subject to competition from RTA binding cluster II MAb SyH7.
[g]See Table 3 for descriptions of families.

however, as none of the ~100 clones that we examined bound to ricin or either of the E12 or G3 peptides (data not shown). The failure to obtain E12- or G3-specific V_HHs was not completely surprising, considering that there are very few examples of single-domain antibodies that recognize linear epitopes, possibly because of the absence of a light chain to provide a cleft for peptide binding (25, 26).

Two final screens were conducted using the HobJo library. Screen 8, which was designed to enrich for V_HHs that bind native (not cryptic) epitopes on RTB, involved panning the HobJo library on RTB captured via ASF (RTB-ASF). The screen gave rise to five unique RTB-specific V_HHs. In screen 9, the V_HH library was panned using two V_HHs identified in screen 1; ricin holotoxin was captured with JIV-F5 to obstruct immunodominant epitopes in cluster I and then saturated with JIV-F6 to mask a subdominant epitope in cluster III (R-F5 + F6). The screen yielded a total of 15 unique V_HHs, including 4 targeting RTA (3 of which were successfully expressed), 8 targeting RTB, and 3 targeting ricin holotoxin.

In total, the nine screens resulted in 68 unique anti-ricin V_HHs: 31 specific for RTA, 33 specific for RTB, and 4 specific for ricin holotoxin (Tables 1 and 2). Fourteen additional V_HHs (7 anti-RTA and 7 anti-RTB) found in various screens were dropped from further study because of their similarity to other V_HHs (i.e., with very few, generally conservative mutations, usually within framework regions) or, in one case, because the V_HH failed to be expressed at sufficiently high levels in *Escherichia coli* to be amenable to analysis (see Table S1 in the supplemental material). The complementarity determining region 3 (CDR3) nucleotide sequences of the entire collection of V_HHs were aligned using BLAST and grouped into families based on length and nucleotide identity. There were nine different clonal families encompassing a total of 24 V_HHs (Tables 2 and 3); the remaining 44 V_HHs were unrelated to each other. The V_HH sequences have been deposited in GenBank (Table 2). Within the group of 68 V_HHs, CDR3 length ranged from 7 to 22 residues, with an average of 14.8 residues.

TABLE 3 V_HH families based on CDR3 similarity[a]

Family[b]	Member(s)	Specificity[c]
JIV-F6	V1B10, **V1D3**	A
JIY-A7	JNM-G4	A
JIY-D9	V2B8	A
V1C7	V2B9, V2E8, **V5C1**	A
V2G10	V1G6	A
JIZ-B7	JIW-D12, JNN-B8, JNN-D1	B
JIW-G10	JNN-A3	B′
V2C11	V2D4, V5H2	B

[a]Bold and underlined data indicate a V_HH with strong TNA; bold data indicate moderate TNA; underlined data indicate weak TNA.
[b]A family was defined as composed of two or more V_HHs having CDR3 sequences of equal lengths and >90% identity at the nucleotide level.
[c]A, RTA; B, RTB; B′, plate-bound RTB.

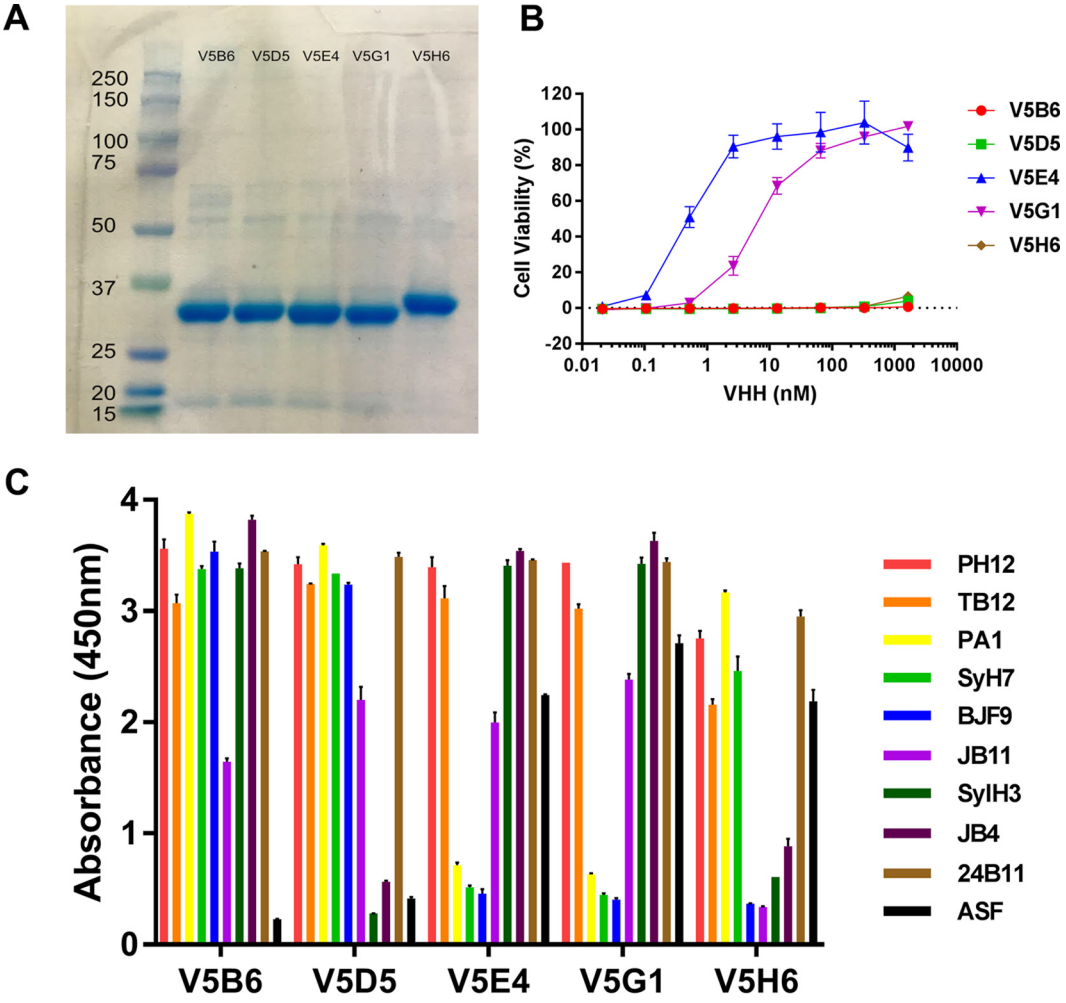

FIG 1 Expression and characterization of ricin-specific V_HHs. All 68 V_HHs in this study (Table 2) were subjected to analysis by SDS-PAGE, toxin-neutralizing assays, and competition ELISA. Data shown here represent results of analysis of five representative RTB-specific V_HHs: V5B6, V5D5, V5E4, V5G1, and V5H6. (A) V_HHs were subjected to SDS-PAGE, and the resulting gel was stained with Coomassie blue. Molecular mass standards (with kilodalton notations) are shown in the far left lane. The major band (~33 to ~35 kDa) in each lane corresponds to the expected molecular mass of the recombinant V_HHs, with an N-terminal thioredoxin fusion partner, a hexa-His tag, and a C-terminal epitope E-tag, as described in the supplemental methods. (B) Toxin-neutralizing activity, as determined in a Vero cell-based microtiter plate assay. The representative set of V_HHs consists of two V_HHs with strong TNA (IC_{50} = <10 nM) and three with no TNA. (C) Competition ELISA, as described in Materials and Methods. Microtiter plates were coated with the indicated MAbs or ASF (legend on right) and then overlaid with ricin. The plates were probed with V_HHs, as indicated along the *x* axis, and were developed with anti-E-tag secondary antibodies. As such, the sandwich ELISA data provided relative competition values against a panel of RTA- and RTB-specific MAbs. The failure of the V_HHs to recognize ricin toxin when bound to ASF is indicative of the antibodies recognizing epitopes near one of the RTB Gal/GalNAc binding sites. The full array of competition ELISAs is presented in Data Set S1.

Classification and characterization of ricin-specific V_HHs. All 68 V_HHs were expressed in *E. coli* as 33- to 35-kDa E-tagged thioredoxin fusion proteins, as described in the supplemental methods and in previous publications (12). The relative purity and integrity of the V_HH preparations were assessed by SDS-PAGE (Fig. 1A). Each of the 68 ricin-specific V_HHs was also assessed for the ability to neutralize ricin toxin in a Vero cell cytotoxicity assay (Fig. 1B and Table 2) (27, 28). Relative 50% inhibitory concentrations (IC_{50}s) were determined by mixing each V_HH at a range of concentrations (0.01 to 10,000 nM) with a fixed amount of ricin before applying it to Vero cells, as described in Materials and Methods. The V_HHs were assigned to one of four groups based on their relative IC_{50}s as follows: <10 nM, strong toxin-neutralizing activity; <100 nM, moderate toxin-neutralizing activity; <500 nM, weak toxin-neutralizing activity; >500 nM, no neutralizing activity. The majority (~80%) had weak (n = 7) or no detectable (n = 47)

TNA, while the remainder (~20%) were evenly divided between strong ($n = 7$) and moderate ($n = 7$) toxin-neutralizing activities (Tables 1 and 2). The results of the toxin-neutralizing assays performed for the 14 V_HHs with strong or moderate TNA are shown in Fig. S2 in the supplemental material. Among the seven V_HHs with the strongest TNA, three were specific for RTA and four were specific for RTB.

V_HH association (K_a) and dissociation (K_d) rates and equilibrium dissociation constants (K_D) for ricin were determined by surface plasmon resonance (SPR) using sensor chips coated with native toxin via amine coupling, as described in Materials and Methods. Kinetic constants were fitted using the Langmuir 1:1 binding model (29). We found that K_D values ranged from 6 pM to ~32 nM (Table 2; see also Table S2 and Fig. S3 in the supplemental material). In general, the V_HHs with the highest binding affinity (K_D) generally had the strongest TNA ($R^2 = 0.6966$; Fig. 2A). For example, all 14 V_HHs with strong and moderate TNA had K_D values of <1 nM, while V_HHs with K_D values of ≥ 1 nM lacked TNA, with one exception. Furthermore, the V_HHs with the strongest TNA also tended to have the slowest off-rates (K_d) ($R^2 = 0.6018$; Fig. 2B), a relationship that has been noted by other investigators (30). The relationship between binding affinity and TNA was most apparent within V_HH clonal families (Fig. 2C), the members of which would be expected to have epitopes similar to each other (31). The failure of antibodies such as JNM-B5 to neutralize ricin despite its relatively high binding affinity (e.g., 60 pM) demonstrates once again that other factors such as epitope specificity contribute to antibody functionality.

Localization of V_HH epitopes on RTA. We next sought to locate the relative binding sites of all V_HHs that recognized soluble ricin, with the expectation that toxin-neutralizing antibodies would segregate into specific bins or clusters of epitopes on RTA and RTB.

We addressed RTA first. In collaboration with Michael Rudolph (New York Structural Biology Center, New York, NY), all 30 RTA-specific V_HHs (excepting JIY-F10, which did not recognize soluble ricin) have been subjected to X-ray crystallography trials. To date, we have reported 10 V_HH-RTA cocrystal structures: 6 that involve epitope cluster I, 3 that involve epitope cluster II, and 1 that straddles clusters I and II (Table 2) (16–18). The two cluster I V_HHs with the strongest TNA, JIY-E5 and JIV-F5, each make considerable contact with RTA's α-helix B (i.e., ~472 to ~477 Å^2), an interaction that has been proposed to be critical for toxin inactivation (17–22, 26, 32). The other cluster I V_HHs, and the cluster I/II V_HH, interacted with β-strand h and α-helix D to various degrees. Within cluster II, the two V_HHs with weak TNA, V1C7 and JIY-E1, made primary contact with α-helices D and E, while V5E1, which has strong TNA, associated with α-helices A and F and the F-G loop. For perspective, we provide a PyMol surface representation of all 10 solved V_HH structures superimposed onto RTA (see Fig. S4 in the supplemental material).

In the absence of additional X-ray crystal structures, epitope localization on RTA was done by competitive sandwich ELISA with a collection of nine different MAbs against epitopes in clusters I (PB10 and WECB2), I and II (SWB1), II (SyH7, PA1, TB12, and PH12), III (IB2), and IV (GD12) (Fig. 3; see also Table S3 in the supplemental material) (19, 20, 53). As described in Materials and Methods, each of the 30 anti-RTA V_HHs was tested for the ability to recognize ricin that had been captured by each of the nine cluster I to IV MAbs. The validity of the sandwich ELISA for epitope mapping was evaluated using the following three V_HHs whose epitopes have been resolved by X-ray crystallography (Fig. 4): JIV-F5 (PDB identifier [ID]: 4Z9K), JIY-D10 (PDB ID: 4LGR), and V1C7 (PDB ID: 5J56) (16–18). In the sandwich ELISA, the binding of JIV-F5 to ricin was affected by PB10, WECB2, and SWB1 but not by SyH7, PA1, PH12, TB12, IB2, or GD12 (Fig. 4A). This competition profile is consistent with the structural epitope of JIV-F5 encompassing α-helix B, β-strand h, and the C-terminal portion of α-helix D (17). By the same token, JIY-D10 was able to bind to ricin that had been captured by GD12, PB10, PA1, SyH7, and IB2 but not WECB2, SWB1, TB12, or PH12, a profile congruent with JIY-D10's structural epitope being localized to α-helices D and E and β-strand h (Fig. 4B). Finally, V1C7 was

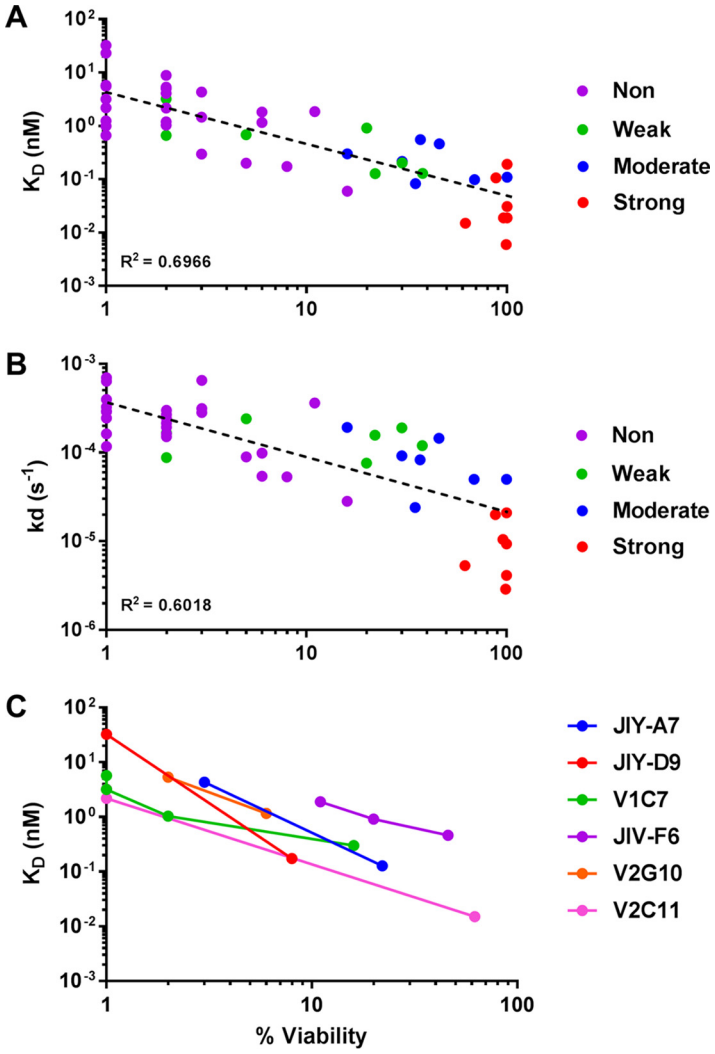

FIG 2 Relationships between V_HH binding affinities and toxin-neutralizing activities. (A and B) Using values presented in Table 2, toxin-neutralizing activity (percent viability at 66 nM V_HH) of representative V_HHs was plotted versus its respective (A) equilibrium dissociation constant (K_D) or (B) off-rate (K_d) value. For simplicity's sake, individual V_HHs are color coded based on their neutralizing activity (i.e., strong, moderate, weak, or no neutralizing [Non] activity). To enable the use of a logarithmic axis, V_HHs that lacked TNA were arbitrarily assigned a value of 1 for percent viability (*x* axis). R^2 values were calculated using the Power Trendline function in Microsoft Excel. (C) TNA as a function of equilibrium dissociation constant (K_D) for the six V_HH clonal families represented in Table 3. Each color represents a family; each dot represents an individual V_HH within that family. The downward slope of the lines suggests a relationship between K_D and TNA within a clonal family (i.e., V_HHs with the highest affinity for ricin also have the strongest TNA). The percentages of cell viability as plotted are from a single representative experiment done in triplicate.

able to bind ricin that had been captured by GD12, PB10, WECB2, and IB2 but not the cluster II-specific MAbs (SyH7, PA1, PH12, and TB12) or the I-II overlap MAb SWB1. This profile is consistent with V1C7 making contact with RTA's α-helix D and α-helix E, along with several additional interactions with loops e-d, C-D, and D-E (16) (Fig. 4C). The sandwich ELISA also successfully positioned the epitopes of the seven additional V_HHs (JIV-G12, JIY-A7, JIY-E1, JIY-E5, JIY-G11, JNM-F8, and V5E1) whose X-ray crystal structures in complex with RTA have been solved (16–18) (see Data Set S1 in the supplemental material). However, it is important to note that the epitope localization determined by the sandwich ELISA is only approximate, as the assay does not discriminate between direct epitope overlap, steric hindrance, and allostery. Indeed, we noted that the sandwich ELISA overestimated V1C7's contact on RTA compared to its known structural epitope as defined by X-ray crystallography (see Fig. S5).

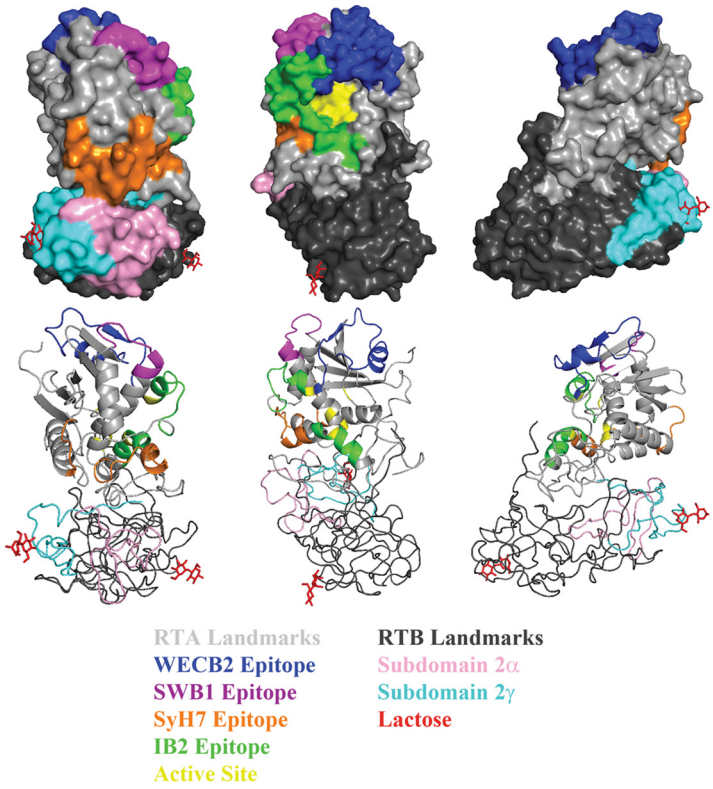

FIG 3 Representative landmarks and functional elements on ricin toxin. Surface (top) and ribbon (bottom) PyMol representations of ricin toxin (PDB ID: 2AAI) at 120° rotations. Landmarks on RTA (gray) include the epitopes recognized by WECB2 (blue), SWB1 (magenta), SyH7 (orange), IB2 (green), and the active site (yellow). Landmarks on RTB (black) include the two galactose binding sites (lactose moieties in red) and subdomains 2α (pink) and 2γ (cyan).

The sandwich ELISA was next used to approximate the binding sites of the remaining 20 RTA-specific V_HHs on the surface of RTA relative to clusters I to IV. All 20 V_HHs were inhibited from binding to ricin by at least one MAb, and the majority (16/20) were inhibited by two or more MAbs (Fig. 5; see also Fig. S6 and Data Set S1 in the supplemental material). In total, the 30 anti-RTA V_HHs fell into 11 different competition profiles, or "bins" (a bin was comprised of all V_HHs which shared the same competition profile). When the bins were aligned vertically and the epitope clusters horizontally, as shown in Fig. 5, it was evident that the putative V_HH binding sites were spatially contiguous across the four previously identified epitope clusters. Moreover, each of the 11 competition bins overlapped WECB2 (cluster I; bins 1 to 6), SyH7 (cluster II; bins 7 and 8), or IB2 (cluster III; bins 9 to 11), suggesting that these three MAbs constitute the immunodominant regions on RTA.

Overall, the competition profiles associated with each of the bins enabled us to assign their location on the surface of RTA with confidence, especially if a bin contained one or more V_HHs whose X-ray crystal structure in complex with RTA has been solved. Bin 2, for example, is defined by competition with PB10, WECB2, and SWB1. These three MAbs have overlapping epitopes on RTA's α-helix B, β-strand h, and α-helix D and the D-E loop (53). Moreover, the structural epitopes of five of the nine V_HHs in bin 2 have been reported (17, 18). Therefore, we can assume that the remaining four V_HHs in bin 2, JIY-E3, JNM-B5, JNM-E4, and JNM-G4, contact α-helix B, β-strand h, and/or α-helix D (Fig. 3; see also Fig. S1).

Similarly, bin 7 is defined by competition with SWB1 and all four cluster II MAbs (PH12, TB12, PA1, and SyH7). PA1 and SyH7 contact the loop before α-helix A and α-helices F and G, while PH12, TB12, and SWB1 contact β-strand d and α-helices D and E. Moreover, as noted above, the structural epitopes of two V_HHs in bin 7, JIY-E1 and V1C7,

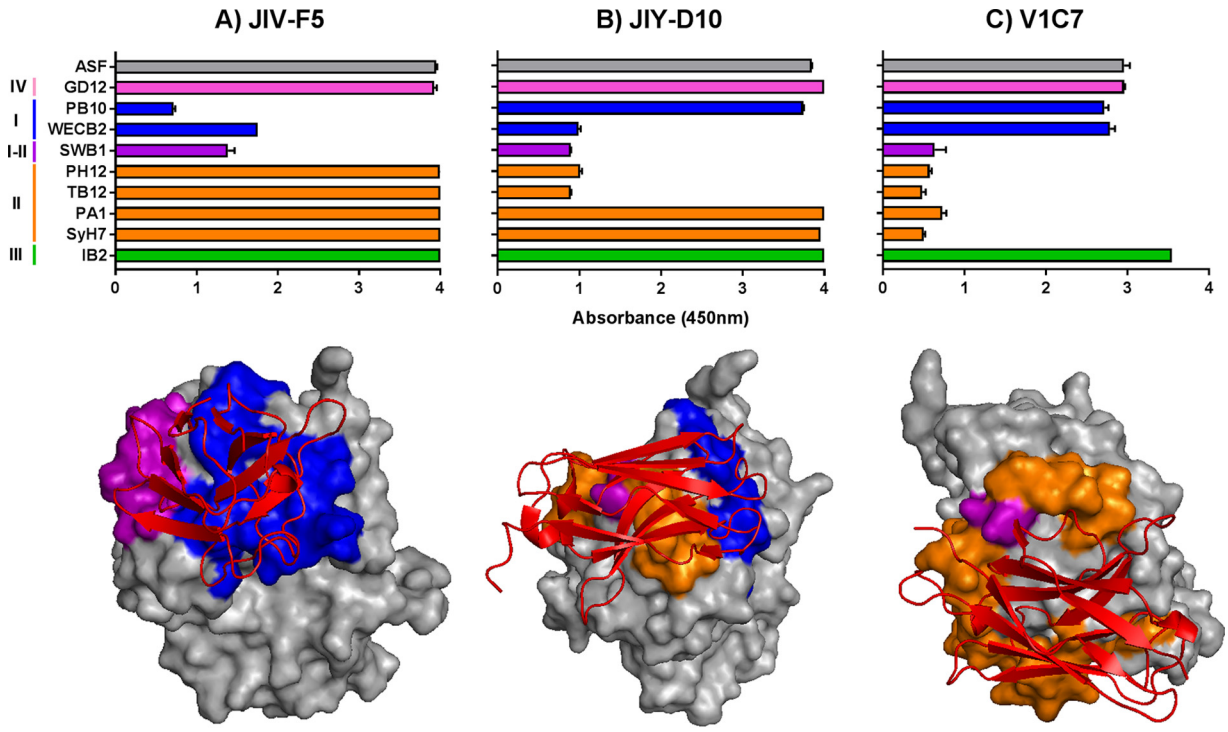

FIG 4 Validation of cross-competition ELISA as a strategy for epitope localization on RTA. (Top panels) V_HHs (A) JIV-F5, (B) JIY-D10, and (C) V1C7 were subjected to competition ELISAs with a panel of RTA-specific MAbs representing neutralizing clusters I to IV, as described in Materials and Methods. As a point of reference, V_HH binding to R-ASF is shown in each panel (gray). (Bottom panels) The known X-ray crystal structures of V_HHs (colored red) (A) JIV-F5, (B) JIY-D10, and (C) V1C7 bound to RTA with relevant murine MAb epitopes (clusters I to IV), color coded as in the top panel. PDB IDs are 4Z9K (JIV-F5), 4LGR (JIY-D10), and 5J56 (V1C7).

have recently been reported (16). The remaining three V_HHs in bin 7, V2B9, V2E8, and V5C1, are members of the V1C7 family (Table 3). Rosetta-based homology modeling suggests that the V1C7 family members, despite their minor differences in CDR sequences, interact with RTA in similar fashions (31). Thus, the epitopes of all five V_HHs in bin 7 can be positioned on RTA with relative accuracy.

In some instances, the results of the sandwich ELISA were more difficult to reconcile. In the case of V1B11 and JNM-D1, representing bins 6 and 10, respectively, considerable cross-cluster competition was involved. V1B11 was competed with by WECB2 (cluster I) and IB2 (cluster III), while JNM-D1 was affected by SyH7 (cluster II) and IB2 (cluster III). When the cross-cluster competition results were taken at face value, the predicted epitopes for V1B11 and JNM-D1 encompassed too large a surface on RTA to localize actual antibody-antigen contact points (Fig. 6). To refine these ambiguous antibody binding sites, we subjected V1B11 and JNM-D1 to epitope mapping by hydrogen-deuterium exchange mass spectrometry (HX-MS), as described recently (31). HX-MS affords peptide-level resolution of antibody binding sites and is therefore an extremely useful methodology for epitope localization (33). As part of this analysis, we also included JNM-C12 (bin 1) since it also demonstrated a degree of cross-cluster competition.

JNM-C12's binding to ricin was inhibited by cluster I (PB10 and WECB2), cluster I/II (SWB1), and cluster IV (GD12) MAbs (Fig. 6A). This profile differs from that seen with bin 2, for which we have several crystal structures, determined solely by competition with cluster IV (GD12). On the basis of this profile, we predicted that JNM-C12's core epitope would encompass RTA's α-helix B and β-strand h and might also potentially include β-strands b to d. This prediction was partially borne out when JNM-C12 was subjected to epitope mapping by HX-MS. Specifically, JNM-C12 strongly protected RTA peptides corresponding to α-helix B (residues 92 to 109) and β-strand h (residues 108 to 122) but did not protect β-strands b to d (see Fig. S7A and Table S5 in the supplemental

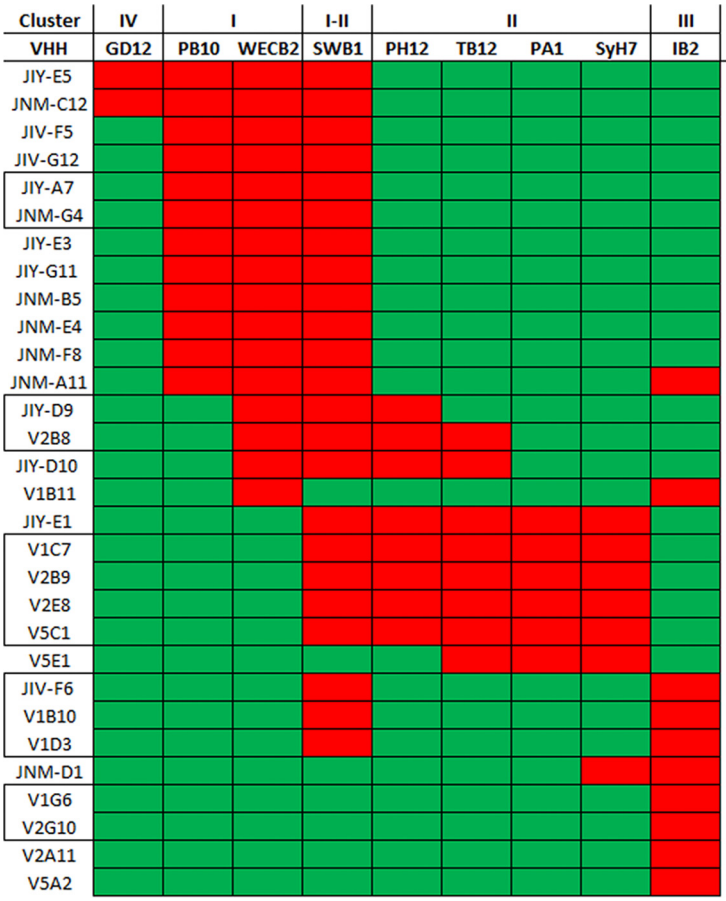

Cluster	IV	I		I-II	II				III			
VHH	GD12	PB10	WECB2	SWB1	PH12	TB12	PA1	SyH7	IB2	Bin	KD (nM)	TNA
JIY-E5										1	0.23	+++
JNM-C12										1	0.099	++
JIV-F5										2	0.019	+++
JIV-G12										2	0.15	+
JIY-A7										2	4.4	-
JNM-G4										2	0.083	+
JIY-E3										2	0.296	-
JIY-G11										2	0.56	++
JNM-B5										2	0.06	-
JNM-E4										2	0.127	++
JNM-F8										2	0.203	+
JNM-A11										3	0.2	-
JIY-D9										4	0.173	-
V2B8										5	32.5	-
JIY-D10										5	0.11	++
V1B11										6	8.87	-
JIY-E1										7	0.69	+
V1C7										7	3.17	-
V2B9										7	1.03	-
V2E8										7	5.73	-
V5C1										7	0.37	++
V5E1										8	0.019	+++
JIV-F6										9	1.89	-
V1B10										9	0.917	+
V1D3										9	0.46	++
JNM-D1										10	1.19	-
V1G6										11	5.33	-
V2G10										11	1.16	-
V2A11										11	1.82	-
V5A2										11	1.46	-

FIG 5 Relative locations of the epitopes recognized by 30 different RTA-specific V_HHs. Thirty RTA-specific V_HHs (left column) were subjected to cross-competition sandwich ELISA with a panel of nine murine MAbs (top row) representing the four different epitope clusters on RTA. Shown here is a binary representation of the actual sandwich ELISA (Fig. S6) in which individual cells are colored red for >50% competition (V_HH versus MAb) and green for <50% competition. V_HH clonal families are boxed (left column). V_HHs with the same competition profile were grouped into bins (right column). For reference, V_HH binding affinities and TNA (from Table 2) are shown in the far right columns.

material). Thus, competition with GD12 may be steric in nature. In this respect, JNM-C12's core epitope involves contact with α-helix B and β-strand h and resembles V_HHs in bin 2.

The sandwich ELISA predicted that JNM-D1 would recognize α-helices C and G and the F-G loop (Fig. 6B). Again, HX-MS analysis partially confirmed this prediction, as JNM-D1 strongly protected peptides encompassing RTA's α-helices C (residues 123 to 135) and G (residues 205 to 210) but not the F-G loop (see Fig. S7B and Table S5 in the supplemental material). On the basis of the sandwich ELISA, V1B11 was predicted to recognize an epitope situated between β-strand h and α-helix C (Fig. 6C). HX-MS analysis of V1B11 revealed that it strongly protected RTA's α-helices C (residues 123 to 135) and G (residues 205 to 210), consistent with the observed IB2 results (see Fig. S7C and Table S5). Thus, HX-MS enabled us to predict with greater confidence the epitopes of V1B11 and JNM-D1 on RTA. Interestingly, despite the differential competition profiles of these two V_HHs, their binding epitopes as determined by HX-MS are almost identical. Thus, the sandwich ELISA may provide additional information regarding the orientation of binding of these V_HHs to that footprint on RTA, which results in differential steric hindrance with WECB2 and SyH7.

HX-MS also revealed another interesting difference between JNM-D1 and V1B11 in residues 249 to 255, which span a 3/10-helix and a β-bridge in RTA's C terminus. This region is on the opposite side of RTA from the residues in helices C and G that are

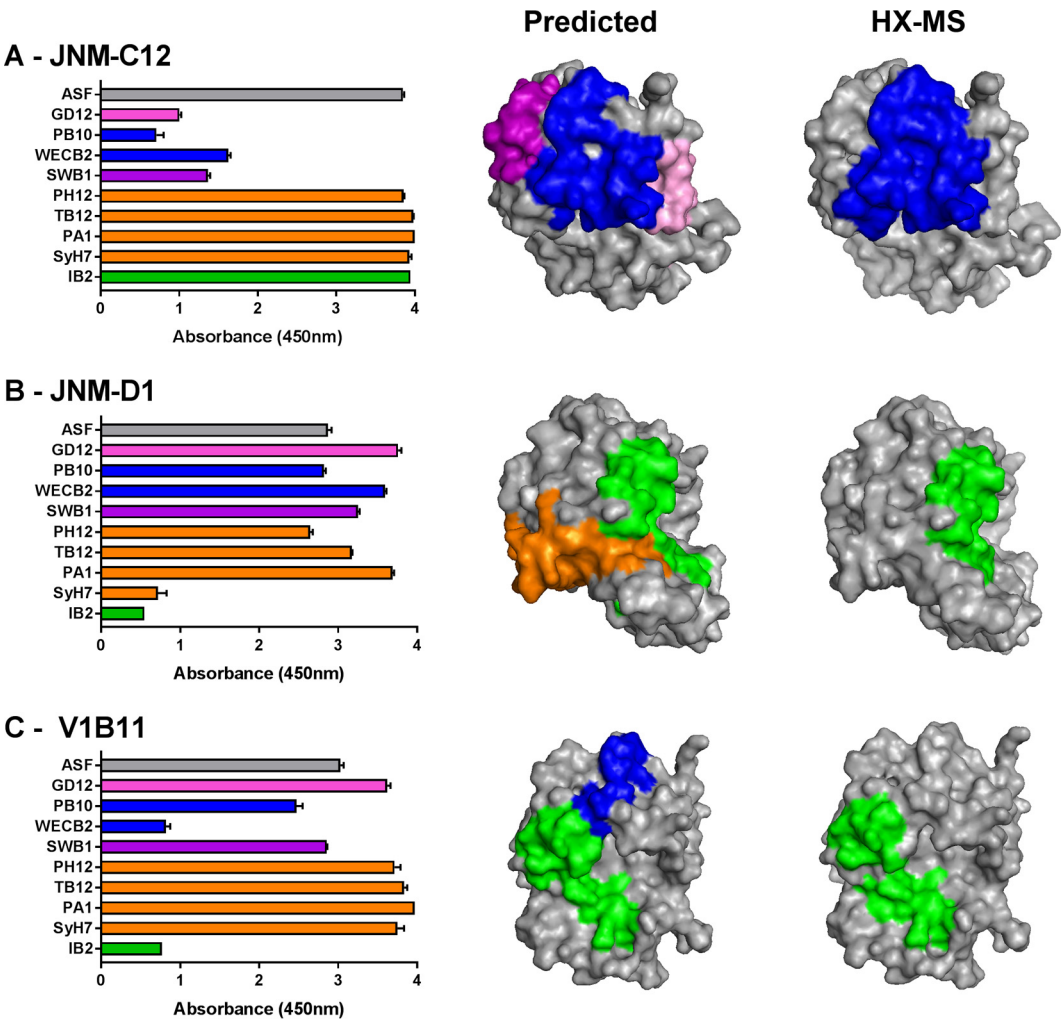

FIG 6 Confirmation of epitope positioning by HX-MS. (Left column) V_HHs (A) JNM-C12, (B) JNM-D1, and (C) V1B11 were subjected to cross-competition ELISAs, as described in the legend to Fig. 4. (Middle column) Based on the competition profiles, the predicted epitopes recognized by JNM-C12, JNM-D1, and V1B11 were positioned on the surface of RTA (PDB ID: 1RTC). (Right column) Results of HX-MS analysis of JNM-C12, JNM-D1, and V1B11 (Fig. S7), mapped onto RTA. The regions of strong protection, shown in the same orientation as in the middle column for comparison, are indicated using cluster-specific colors.

strongly protected by both V_HHs and would not be exposed to solvent in the context of ricin holotoxin. While JNM-D1 induced strong deprotection (i.e., increased flexibility leading to faster hydrogen exchange) in this region, V1B11 induced strong protection (see Fig. S7B and C in the supplemental material). We hesitate to speculate about the significance of the observed deprotection/protection associated with RTA's C terminus, considering that this region of RTA is prone to unfolding in the absence of RTB. Nonetheless, the observation that two V_HHs (JNM-D1 and V1B11) with seemingly identical binding sites (and similar affinities) have opposite effects (protection versus deprotection) on RTA's C terminus raises interesting questions about potential allosteric changes that can occur within the context of ricin toxin.

Spatial location and secondary elements on RTA associated with neutralizing epitopes. We had originally proposed that toxin-neutralizing antibodies would be confined to a very limited number of sites on RTA, a hypothesis that proved to be somewhat accurate. As shown in Fig. 5, although V_HHs with strong and moderate TNA were distributed across six different bins (namely, bins 1, 2, 5, 7, 8, and 9), the six bins likely constitute two hot spots. One hot spot, defined by competition with WECB2 and SWB1 and represented by JNM-C12, JIV-F5, and JIY-D10, among others, involves α-helix B and possibly the C-terminal portion of α-helix D (Fig. 3; see also Fig. S1) (17, 18).

Although β-strand h sits between these structural elements, evidence provided by X-ray crystal structure analysis suggests that the interaction with strand h alone is not sufficient to confer TNA (17, 18). The other hot spot, defined by competition with SyH7 and PA1 and represented by V5E1, involves contact with the loop preceding α-helix A, α-helix F itself, and the F-G loop, with the F-G loop likely the critical determinant of strong neutralizing activity (16).

With that in mind, we can account, at the structural level, for strong and moderate TNA associated with other RTA-specific V_HHs. V_HHs in bins 1 to 6 with detectable TNA (e.g., JNM-E4) would be predicted to engage with α-helix B and/or α-helix D, while V_HHs in bins 7 and 8 would be expected to contact α-helix F and the F-G loop. V5C1 (bin 7) sits between these two hot spots, being competed with by all three of SWB1 and SyH7/PA1, and thus may neutralize via contact with either or both hot spots. V1D3 (bin 9) is interesting because it is competitively inhibited by both IB2 and SWB1. On the basis of this profile, V1D3 would be expected to make contact with α-helices C and G and/or the C-terminal portion of α-helix D. Its neutralizing activity may therefore be due to contact with α-helix D and/or proximity to the F-G loop. Alternatively, it may represent a third neutralizing hot spot associated with α-helix C.

The story is more complicated, however, because even among V_HHs with identical competition profiles there were often disparities in TNA that are explained only partially by binding affinities (K_D). In bin 2, for example, JIV-F5, JNM-B5, and JNM-G4 have identical competition profiles and similar binding affinities (0.02 nM, 0.06 nM, and 0.128 nM, respectively) but very different neutralizing activities; JNM-B5 lacks TNA, JNM-G4 has weak TNA, and JIV-F5 has strong TNA. On the basis of the six reported structural epitopes in this area of RTA (17, 18), we hypothesize that JNM-B5 engages solely with β-strand h and not with α-helix D or α-helix B. CDR3 of JIV-F5 is relatively short (16 residues) and contains a disulfide bond between Cys50 and Cys97 that renders it spatially constrained; we previously showed that its short length and constrained conformation prevent the formation of an intermolecular β-sheet with β-strand h (17). In contrast, JNM-B5 and JNM-G4 have longer CDR3 sequences (19 and 22 residues, respectively) that are devoid of the cysteine residues necessary for disulfide bond formation. In this respect, JNM-B5 and JNM-G4 resemble JIY-G11 (PDB ID: 4LHJ), JIY-A7 (PDB ID: 4LHQ), and JIV-G12 (PDB ID: 4LGS), whose unconstrained CDR3 elements form strand-strand interactions with β-strand h. However, definitive conclusions about the actual contact points for JNM-B5 and JNM-G4 on RTA await HX-MS and/or X-ray crystal structure analysis.

Epitope localization of toxin-neutralizing and nonneutralizing RTB- and ricin holotoxin-specific V_HHs. We next turned our attention to the 20 V_HHs isolated from the HobJo library that were RTB or holotoxin specific and that could bind to soluble ricin. Using a sandwich ELISA with five benchmark anti-RTB MAbs (see Table S4 in the supplemental material), four RTA-specific cluster II MAbs (SyH7, PA12, PH12, and TB12), and the surrogate receptor, ASF, we tentatively localized the epitopes recognized by 16 of the RTB- and holotoxin-specific V_HHs (Fig. 1C and 7; see also Fig. S8 and Data Set S1). Four V_HHs were unaffected by the panel of MAbs used in the sandwich ELISA, indicating that they recognize epitopes situated outside our existing panel of MAbs.

The 16 RTB- and holotoxin-specific V_HHs constituted 12 different bins, based on their competition profiles in the sandwich ELISA. The 11 V_HHs in bins 1 to 7 shared the common trait, in the sandwich ELISA, of being inhibited by PA1 and SyH7, a finding that has important implications for epitope localization on RTB. SyH7 and PA1 each make contact with RTA near the interface with RTB's subdomains 2α (residues 148 to 183) and 2γ (residues 228 to 262) (Fig. 3) (53). We would predict, therefore, that all 11 V_HHs in bins 1 to 7 recognize epitopes within RTB's subdomains 2α and/or 2γ and that the observed competition with SyH7 and PA1 in the sandwich ELISA is due to steric hindrance. V_HHs in bins 1 to 3 would be predicted to bind epitopes abutting the RTA-RTB interface, based on the observed competition with TB12 and PH12, whose epitopes are considerably "north" of the border. In fact, V5D1, V5G12, and V1B4 (comprising all of bins 1 and 2) bind ricin holotoxin, but not the individual subunits,

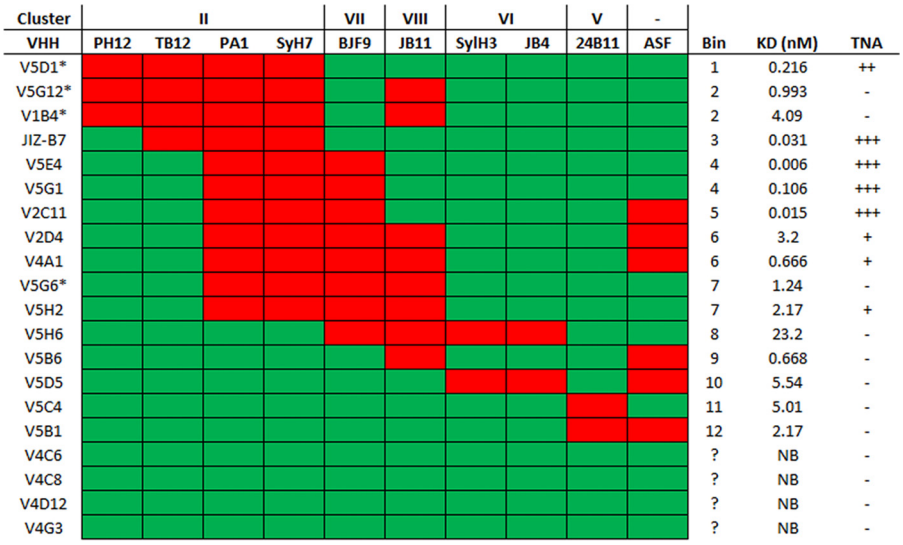

FIG 7 Relative locations of the epitopes recognized by holotoxin- or RTB-specific V_HHs. Twenty holotoxin (*)- or RTB-specific V_HHs (left column) were subjected to cross-competition sandwich ELISA with a panel of nine murine MAbs and ASF (top row). Shown here is a binary representation of the actual sandwich ELISA (Fig. S8) in which individual cells are colored red for >50% competition (V_HH versus MAb) and green for <50% competition. V_HHs with the same competition profile were grouped together into bins (right column). For reference, V_HH binding affinity data and TNA data (from Table 2) are shown in the far right columns.

indicating that they recognize quaternary epitopes that straddle the RTA-RTB interface. Finally, based on the observed competition with ASF, V_HHs in bins 5 and 6 are predicted to have epitopes situated in close proximity to (or even overlapping) the Gal/GalNAc recognition element in subdomain 2γ (Fig. 3). Elsewhere, we report results of extensive cross-competition studies performed to refine the epitopes on RTB's domain 2 recognized by the 11 V_HHs in bins 1 to 7 (A. Y. Poon, D. Vance, Y. Rong, D. Ehrbar, and N. Mantis, unpublished data).

Bins 8 to 12 each contained a single V_HH. On the basis of competition with SylH3 and JB4, we would propose that V5H6 (bin 8) and V5D5 (bin 10) also recognize epitopes in RTB domain 2. Moreover, the fact that V5D5 is unable to recognize R-ASF suggests that its epitope is occluded upon RTB-receptor interaction and is therefore in close proximity to the Gal/GalNAc recognition domain but on the opposite side from V_HHs in bins 5 and 6. In contrast, V5C4 (bin 11) and V5B1 (bin 12) were each competitively inhibited from binding to ricin by 24B11, which is postulated to recognize RTB subdomain 1 (34–36). V5B1 was also unable to recognize R-ASF, presumably because its epitope is near the domain 1 Gal-specific binding element (5). We recently identified three additional MAbs specific for RTB's domain 1, although they were not included in this study (37).

Among the 20 RTB- and holotoxin-specific V_HHs isolated from the HobJo library, four were classified as having strong TNA, one moderate TNA, and three weak TNA (Fig. 7 and Table 2). The four V_HHs with strong TNA had K_D values of <110 pM and were located in bins 3 (JIZ-B7), 4 (V5E4 and V5G1), and 5 (V2C11). They are also defined by competition with the two anti-RTA MAbs, SyH7 and PA1. On the basis of their competition profiles, we hypothesize that JIZ-B7, V5E4, V5G1, and V2C11 recognize a neutralizing hot spot at the RTA-RTB interface. Two V2C11 family members, V2D4 and V5H2, are also predicted to target this hot spot but have only weak TNA, probably because of their relatively low binding affinities.

Along those same lines, it should be underscored that V5E1 and JIZ-B7 have identical competition profiles, even though V5E1 is classified as an RTA-specific antibody and JIZ-B7 as an RTB-specific antibody (Fig. 5 and 7). Had we conducted the epitope binning studies with ricin holotoxin rather than the individual RTA and RTB

subunits, V5E1 and JIZ-B7 would theoretically have been in the same bin. We speculate that JIZ-B7 recognizes a quaternary epitope that straddles the RTA-RTB border, possibly even in a configuration that mirrors V5E1 (16).

DISCUSSION

In this study, we sought to advance our longstanding efforts to generate a comprehensive B cell epitope map of ricin toxin with a focus on localizing the epitopes recognized by toxin-neutralizing antibodies. Ricin's enzymatic subunit (RTA) is of particular interest to the biodefense research community as two recombinant RTA-based vaccines, RiVax and RV*Ec*, are being evaluated in preclinical and clinical studies (38–40). Predicting the efficacy of these two vaccine candidates in humans is challenging, because neither the anti-ricin serum IgG titer nor the TNA is necessarily a reliable predictor of protective immunity (41). However, there is evidence that epitope-specific antibody responses may be more useful measures in this regard (42). The availability of a high-resolution epitope map of RTA would enable a targeted analysis of specific antibody responses following vaccination, possibly even resulting in the identification of a serum antibody profile that correlates with immunity. Understanding the antibody response to RTA is also relevant to the development of RTA-based immunotoxins, whose efficacy (in some instances) has been limited by the onset of one or more toxin-neutralizing antibodies that render the immunotoxin inactive (43, 44).

We estimate that the current collection of 68 V_HHs described in this study covers slightly more than 50% of the surface area of RTA, with a particular bias toward two immunodominant regions of RTA, referred to as epitope clusters I and II (20). Areas not covered in the current V_HH repertoire include the entire "backside" of RTA (Fig. 3, right panel; see also Fig. S1 in the supplemental material). In terms of RTB, we identified an aggregate of neutralizing epitopes localized at the RTA-RTB interface positioned in close proximity to the Gal/GalNAc recognition element of RTB's domain 2γ (5). In a separate report, we refer to this region of RTB as "supercluster II" and demonstrate that toxin-neutralizing activity is associated with antibody binding in the vicinity of the RTA-RTB interface (as manifested through competition ELISA performed with SyH7 and V5E1) rather than with obstruction of the Gal/GalNAc recognition element (A. Y. Poon, D. Vance, Y. Rong, D. Ehrbar, and N. Mantis, unpublished data). This interfacial region of ricin toxin is also apparently the target of a number of holotoxin-specific V_HHs (e.g., V5D1) whose epitopes likely involve residues on both sides of the border. Unfortunately, our current report does not address the mechanism(s) by which the supercluster II antibodies neutralize ricin. We can only speculate that they interfere with a region of the toxin that is required for retrograde transport from the plasma membrane to the ER and/or retrotranslocation from the ER to the cytoplasm (45–48).

Nonetheless, our results are consistent with there being two putative neutralizing hot spots on RTA, with "hot spot" being defined as a cluster of closely spaced epitopes recognized by antibodies with potent toxin-neutralizing activity. The first hot spot encompasses RTA's α-helix B and α-helix D. The importance of α-helix B as a target of neutralizing antibodies has been recognized for more than 2 decades (22, 49), although it is only recently that the critical holdfasts have been identified (16, 18, 21, 26, 32). The second hot spot (as noted above) is located at the RTA-RTB interface, defined by RTA's α-helix F and the F-G loop and (possibly) RTB's subdomains 2α and/or 2γ (16). At present, it is not clear why these regions render ricin vulnerable to antibody attack, although evidence is mounting that neutralization occurs intracellularly rather than extracellularly (13, 45–47).

The HobJo V_HHs described here should be a valuable resource for the ricin toxin research community and may have important applications not only for vaccine development but also for diagnostics and therapeutics. For example, Turner et al. recently showed that pairing a llama-derived anti-ricin V_HH (D12fneg) with a modified version of alpaca-derived V_HH JIV-F6 (F6m+) yielded a highly sensitive assay that could detect less than 1 ng/ml of ricin (12, 50). Here we have described two new JIV-F6 family members, V1B10 and V1D3, each with higher affinities for ricin than JIV-F6. In another

application, Legler et al. used JIV-F6, JIY-D10, and JIY-E1, along with several of their own anti-ricin V_HHs, to show that the ability of a V_HH to increase the melting temperature of RTA correlated with its neutralization ability (26). The availability of dozens of additional V_HH coding sequences, affinities, and TNAs (Table 2) enables those types of analyses to be extended. Finally, the V_HHs are amenable to recombinant engineering and may provide a platform for therapeutic development. We demonstrated, for example, that select V_HH heterodimers effectively aggregate ricin in solution and inactive the toxin *in vitro* and *in vivo* (12–14). With the available epitope maps derived from the current study, it is now possible to rationally design different V_HH bispecific antibodies with appropriate linkers intended to target notable hot spots on RTA and RTB.

MATERIALS AND METHODS

Ricin-specific V_HH phage display library. The single-domain-antibody (V_HH) library has been described previously (12). The library is referred to as "HobJo" here in reference to the names of the two immunized alpacas, Hobbs and Johnnes. The V_HH-pIII phagemid library was maintained in *E. coli* TG1 at −80°C. The library was subjected to nine different screens, as described in Table 1 and in Results. Each screen consisted of low-stringency (round 1) and high-stringency (round 2) panning procedures in which target antigen was present at 10 μg/ml and 1 μg/ml, respectively. To begin each screen, an aliquot of the library was used to inoculate Super Broth (SB) medium supplemented with 100 μg/ml ampicillin and 2% glucose. The culture was grown at 37°C to an absorbance at 600 nm (OD_{600}) of ~0.6 to ~0.8 and then infected with VCSM13 helper phage carrying kanamycin resistance (Agilent Technologies, Santa Clara, CA). After a 2-h infection at 37°C, the bacteria were pelleted at 8,000 rpm, reconstituted in SB medium supplemented with ampicillin (100 μg/ml), kanamycin (70 μg/ml), and 0.1% glucose, and incubated overnight at 30°C. The next morning, the bacteria were pelleted by centrifugation and discarded. The resulting supernatants containing V_HH-displaying phages were precipitated with 1:5 (vol/vol) 20% polyethylene glycol (PEG 8000)–2.5 M NaCl at 4°C for 2 h. The supernatant was subjected to centrifugation at 8,000 rpm for 20 min to pellet the phages, which were then resuspended in phosphate-buffered saline (PBS) and used for round 1 of panning. Further phage panning protocols are presented in detail in the supplemental material. Chosen V_HHs were expressed as fusion proteins with an N-terminal thioredoxin tag, a linker containing a hexa-His purification tag, and a C-terminal epitopic E-tag (GAPVP YPDPLEPR) in *E. coli* Rosetta-gami 2(DE3)pLacI (EMD Millipore, Billerica, MA) as previously described (14, 15) and presented in detail in the supplemental material.

Peptides. Biotin-tagged peptides E12 (HPDNQEDAEAITHLFTDV) and G3 (IEGEMRTRIRYNRRSAPD) used in screen 7 were synthesized by Genemed Synthesis, Inc. (San Antonio, TX).

ELISA. For cross-competition sandwich ELISAs, Nunc microtiter plates were coated with competitor capture MAbs (1 μg/ml in PBS) or ASF (4 μg/ml in PBS) overnight at 4°C and then blocked for 2 h with 2% goat serum–0.1% Tween 20 phosphate-buffered saline (PBST). Ricin (1 μg/ml), RTA (0.5 μg/ml), or RTB (0.5 μg/ml) was then captured by the MAbs or ASF and probed with V_HH analytes at 330 nM. Bound V_HHs were detected with an anti-E tag–horseradish peroxidase (HRP) secondary antibody (Bethyl Labs, Montgomery, TX) and developed with SureBlue TMB (3,3′,5,5′-tetramethylbenzidine) substrate (KPL). After quenching was performed with 1 M phosphoric acid, absorbance was read at 450 nm on a VersaMax microplate reader (Molecular Devices, Sunnyvale, CA).

Vero cell cytotoxicity assays. Relative $IC_{50}s$ were determined in Vero cell cytotoxicity assays, as previously described (28). Vero cells were detached from culture dishes with trypsin, adjusted to ~5×10^4 cells per ml, seeded (100 μl/well) into white 96-well plates (Corning Life Sciences, Corning, NY), and allowed to adhere overnight. The cells were then treated with ricin (0.01 μg/ml; 154 pM), ricin-V_HH mixtures, or medium alone (negative control) for 2 h at 37°C. The cells were washed and then incubated for 48 h at 37°C, after which cell viability was assessed using CellTiter-GLO (Promega, Madison, WI). All treatments were performed in triplicate. Relative $IC_{50}s$ were determined following published guidelines in which 100% viability was derived from cells treated with medium only, while 0% viability was defined as the average value obtained from ricin-treated cells (51). Reported relative $IC_{50}s$ for each V_HH were derived from at least three independent toxin-neutralizing assays (each done in triplicate).

SPR and affinity determinations. V_HH association and dissociation rates for ricin toxin were determined by surface plasmon resonance (SPR) using a ProteOn XPR36 system (Bio-Rad Inc., Hercules, CA), as described previously (18, 37). For ricin immobilization, general layer compact (GLC) chips were equilibrated in running buffer (PBS–0.005% Tween) at a flow rate of 30 μl/min. Following EDAC [N-ethyl-N′-(3-dimethylaminopropyl) carbodiimide hydrochloride] (200 mM)–sulfo-NHS (N-hydroxysulfosuccinimide) (50 mM) activation (3 min), ricin was diluted in 10 mM sodium acetate (pH 5.0) at either 4 μg/ml or 2 μg/ml and coupled for 2 min. A third vertical channel received only acetate buffer and served as a reference channel. The surfaces were deactivated using 1 M ethanolamine for 5 min. A ProteOn array system multichannel module (MCM) was rotated to the horizontal orientation for affinity determination experiments. Each V_HH was serially diluted in running buffer and then injected at 50 μl/min for 180 s, followed by 1 to 3 h of dissociation. After each experiment, the chip was regenerated with 10 mM glycine (pH 1.5) at 100 μl/min for 18 s, until the response unit (RU) values had returned to baseline. All kinetic experiments were performed at 25°C. Kinetic constants for the antibody/ricin interactions were obtained with ProteOn Manager software 3.1.0 (Bio-Rad Inc.) using the Langmuir fit model.

Epitope mapping by hydrogen deuterium exchange-mass spectrometry (HX-MS). The HX-MS method for epitope mapping V_HH antibodies is described in more detail elsewhere (R. Toth IV and D. D. Weis, unpublished results) (31). For safety reasons, epitope mapping studies were conducted with a nontoxic variant of RTA known as RiVax (52). Briefly, regions of RiVax where the rate of HX was significantly lower (protection) or higher (deprotection) in the presence of bound V_HH were identified using k-means clustering and significance testing based on time-averaged HX measurements ($\Delta\overline{HX}$). However, unlike that previous work, here the results were not filtered for the solvent accessibility of the RiVax residues. Using k-means clustering, the regions that were assigned as showing strong and intermediate protection were used to define the epitope. The RiVax peptides are numbered sequentially from the N terminus to the C terminus and described in Table S5 in the supplemental material.

Molecular graphics. Images of ricin holotoxin (PBD ID: 2AAI), RTA (PDB ID: 1RTC), and RTA-V_HH complexes (see Table 2 for PDB IDs) were generated using PyMOL (The PyMOL Molecular Graphics System; Schrodinger LLC, San Diego, CA).

Accession number(s). All V_HH nucleotide sequences were deposited into GenBank (see Table 2) and the Immune Epitope Database (IEDB) (pending).

SUPPLEMENTAL MATERIAL

Supplemental material for this article may be found at https://doi.org/10.1128/CVI.00236-17.

SUPPLEMENTAL FILE 1, PDF file, 3.6 MB.

SUPPLEMENTAL FILE 2, XLSX file, 0.1 MB.

ACKNOWLEDGMENTS

We thank Amanda Poon (University at Albany), Greta Van Slyke (Wadsworth Center), and Michael Rudolph (New York Structural Biology Center) for technical assistance with epitope mapping studies. We thank the Wadsworth Center's Applied Genomics Technology Core for DNA sequencing and the Biochemistry/Immunology Core facility for access to SPR instrumentation.

Research reported in this work was supported by contract no. HHSN272201400021C from the National Institutes of Allergy and Infectious Diseases, National Institutes of Health. The content is solely the responsibility of the authors and does not necessarily represent the official views of the National Institutes of Health. The funders had no role in study design, data collection and analysis, decision to publish, or preparation of the manuscript.

REFERENCES

1. Schrot J, Weng A, Melzig MF. 2015. Ribosome-inactivating and related proteins. Toxins (Basel) 7:1556–1615. https://doi.org/10.3390/toxins7051556.
2. Endo Y, Mitsui K, Motizuki M, Tsurugi K. 1987. The mechanism of action of ricin and related toxic lectins on eukaryotic ribosomes. The site and the characteristics of the modification in 28 S ribosomal RNA caused by the toxins. J Biol Chem 262:5908–5912.
3. Endo Y, Tsurugi K. 1987. RNA N-glycosidase activity of ricin A-chain. Mechanism of action of the toxic lectin ricin on eukaryotic ribosomes. J Biol Chem 262:8128–8130.
4. Tesh VL. 2012. The induction of apoptosis by Shiga toxins and ricin. Curr Top Microbiol Immunol 357:137–178.
5. Rutenber E, Ready M, Robertus JD. 1987. Structure and evolution of ricin B chain. Nature 326:624–626. https://doi.org/10.1038/326624a0.
6. Sandvig K, Olsnes S, Pihl A. 1976. Kinetics of binding of the toxic lectins abrin and ricin to surface receptors of human cells. J Biol Chem 251:3977–3984.
7. Sandvig K, Skotland T, van Deurs B, Klokk TI. 2013. Retrograde transport of protein toxins through the Golgi apparatus. Histochem Cell Biol 140:317–326. https://doi.org/10.1007/s00418-013-1111-z.
8. Spooner RA, Lord JM. 2012. How ricin and Shiga toxin reach the cytosol of target cells: retrotranslocation from the endoplasmic reticulum. Curr Top Microbiol Immunol 357:19–40. https://doi.org/10.1007/82_2011_154.
9. Reisler RB, Smith LA. 2012. The need for continued development of ricin countermeasures. Adv Prev Med 2012:149737. https://doi.org/10.1155/2012/149737.
10. Wolfe DN, Florence W, Bryant P. 21 February 2013. Current biodefense vaccine programs and challenges. Hum Vaccin Immunother https://doi.org/10.4161/hv.24063.
11. Pincus SH, Bhaskaran M, Brey RN, III, Didier PJ, Doyle-Meyers LA, Roy CJ. 2015. Clinical and pathological findings associated with aerosol exposure of macaques to ricin toxin. Toxins (Basel) 7:2121–2133. https://doi.org/10.3390/toxins7062121.
12. Vance DJ, Tremblay JM, Mantis NJ, Shoemaker CB. 2013. Stepwise engineering of heterodimeric single domain camelid V_HH antibodies that passively protect mice from ricin toxin. J Biol Chem 288:36538–36547. https://doi.org/10.1074/jbc.M113.519207.
13. Herrera C, Klokk TI, Cole R, Sandvig K, Mantis NJ. 2016. A bispecific antibody promotes aggregation of ricin toxin on cell surfaces and alters dynamics of toxin internalization and trafficking. PLoS One 11:e0156893. https://doi.org/10.1371/journal.pone.0156893.
14. Herrera C, Tremblay JM, Shoemaker CB, Mantis NJ. 2015. Mechanisms of ricin toxin neutralization revealed through engineered homodimeric and heterodimeric camelid antibodies. J Biol Chem 290:27880–27889. https://doi.org/10.1074/jbc.M115.658070.
15. Herrera C, Vance DJ, Eisele LE, Shoemaker CB, Mantis NJ. 2014. Differential neutralizing activities of a single domain camelid antibody (V_HH) specific for ricin toxin's binding subunit (RTB). PLoS One 9:e99788. https://doi.org/10.1371/journal.pone.0099788.
16. Rudolph MJ, Vance DJ, Cassidy MS, Rong Y, Mantis NJ. 2017. Structural analysis of single domain antibodies bound to a second neutralizing hot spot on ricin toxin's enzymatic subunit. J Biol Chem 292:872–883. https://doi.org/10.1074/jbc.M116.758102.
17. Rudolph MJ, Vance DJ, Cassidy MS, Rong Y, Shoemaker CB, Mantis NJ. 2016. Structural analysis of nested neutralizing and non-neutralizing B cell epitopes on ricin toxin's enzymatic subunit. Proteins 84:1162–1172. https://doi.org/10.1002/prot.25062.
18. Rudolph MJ, Vance DJ, Cheung J, Franklin MC, Burshteyn F, Cassidy MS, Gary EN, Herrera C, Shoemaker CB, Mantis NJ. 4 June 2014. Crystal

structures of ricin toxin's enzymatic subunit (RTA) in complex with neutralizing and non-neutralizing single-chain antibodies. J Mol Biol https://doi.org/10.1016/j.jmb.2014.05.026.
19. O'Hara JM, Neal LM, McCarthy EA, Kasten-Jolly JA, Brey RN, III, Mantis NJ. 2010. Folding domains within the ricin toxin A subunit as targets of protective antibodies. Vaccine 28:7035–7046. https://doi.org/10.1016/j.vaccine.2010.08.020.
20. O'Hara JM, Kasten-Jolly JC, Reynolds CE, Mantis NJ. 2014. Localization of non-linear neutralizing B cell epitopes on ricin toxin's enzymatic subunit (RTA). Immunol Lett 158:7–13. https://doi.org/10.1016/j.imlet.2013.11.009.
21. Vance DJ, Mantis NJ. 2012. Resolution of two overlapping neutralizing B cell epitopes within a solvent exposed, immunodominant alpha-helix in ricin toxin's enzymatic subunit. Toxicon 60:874–877. https://doi.org/10.1016/j.toxicon.2012.06.014.
22. Lebeda FJ, Olson MA. 1999. Prediction of a conserved, neutralizing epitope in ribosome-inactivating proteins. Int J Biol Macromol 24:19–26. https://doi.org/10.1016/S0141-8130(98)00059-2.
23. Friguet B, Djavadi-Ohaniance L, Goldberg ME. 1984. Some monoclonal antibodies raised with a native protein bind preferentially to the denatured antigen. Mol Immunol 21:673–677. https://doi.org/10.1016/0161-5890(84)90053-1.
24. Jemmerson R. 1987. Antigenicity and native structure of globular proteins: low frequency of peptide reactive antibodies. Proc Natl Acad Sci U S A 84:9180–9184. https://doi.org/10.1073/pnas.84.24.9180.
25. De Genst E, Silence K, Decanniere K, Conrath K, Loris R, Kinne J, Muyldermans S, Wyns L. 2006. Molecular basis for the preferential cleft recognition by dromedary heavy-chain antibodies. Proc Natl Acad Sci U S A 103:4586–4591. https://doi.org/10.1073/pnas.0505379103.
26. Legler PM, Compton JR, Hale ML, Anderson GP, Olson MA, Millard CB, Goldman ER. 2017. Stability of isolated antibody-antigen complexes as a predictive tool for selecting toxin neutralizing antibodies. MAbs 9:43–57. https://doi.org/10.1080/19420862.2016.1236882.
27. Konowalchuk J, Speirs JI, Stavric S. 1977. Vero response to a cytotoxin of Escherichia coli. Infect Immun 18:775–779.
28. Wahome PG, Mantis NJ. 2013. High-throughput, cell-based screens to identify small-molecule inhibitors of ricin toxin and related category B ribosome inactivating proteins (RIPs). Curr Protoc Toxicol 2013:Chapter 2:Unit 2.23. https://doi.org/10.1002/0471140856.tx0223s55.
29. O'Shannessy DJ, Brigham-Burke M, Soneson KK, Hensley P, Brooks I. 1993. Determination of rate and equilibrium binding constants for macromolecular interactions using surface plasmon resonance: use of nonlinear least squares analysis methods. Anal Biochem 212:457–468. https://doi.org/10.1006/abio.1993.1355.
30. Rosenfeld R, Alcalay R, Mechaly A, Lapidoth G, Epstein E, Kronman C, S JF, Mazor O. 3 May 2017. Improved antibody-based ricin neutralization by affinity maturation is correlated with slower off-rate values. Protein Eng Des Sel https://doi.org/10.1093/protein/gzx028.
31. Bazzoli A, Vance DJ, Rudolph MJ, Rong Y, Angalakurthi SK, Toth RT, IV, Middaugh CR, Volkin DB, Weis DD, Karanicolas J, Mantis NJ. 4 August 2017. Using homology modeling to interrogate binding affinity in neutralization of ricin toxin by a family of single domain antibodies. Proteins https://doi.org/10.1002/prot.25353.
32. Dai J, Zhao L, Yang H, Guo H, Fan K, Wang H, Qian W, Zhang D, Li B, Wang H, Guo Y. 2011. Identification of a novel functional domain of ricin responsible for its potent toxicity. J Biol Chem 286:12166–12171. https://doi.org/10.1074/jbc.M110.196584.
33. Brown KA, Wilson DJ. 13 July 2017. Bottom-up hydrogen deuterium exchange mass spectrometry: data analysis and interpretation. Analyst https://doi.org/10.1039/c7an00662d.
34. McGuinness CR, Mantis NJ. 2006. Characterization of a novel high-affinity monoclonal immunoglobulin G antibody against the ricin B subunit. Infect Immun 74:3463–3470. https://doi.org/10.1128/IAI.00324-06.
35. Yermakova A, Mantis NJ. 2011. Protective immunity to ricin toxin conferred by antibodies against the toxin's binding subunit (RTB). Vaccine 29:7925–7935. https://doi.org/10.1016/j.vaccine.2011.08.075.
36. Yermakova A, Vance DJ, Mantis NJ. 2012. Sub-domains of ricin's B subunit as targets of toxin neutralizing and non-neutralizing monoclonal antibodies. PLoS One 7:e44317. https://doi.org/10.1371/journal.pone.0044317.
37. Rong Y, Van Slyke G, Vance DJ, Westfall J, Ehrbar D, Mantis NJ. 2017. Spatial location of neutralizing and non-neutralizing B cell epitopes on domain 1 of ricin toxin's binding subunit. PLoS One 12:e0180999. https://doi.org/10.1371/journal.pone.0180999.
38. Pittman PR, Reisler RB, Lindsey CY, Guerena F, Rivard R, Clizbe DP, Chambers M, Norris S, Smith LA. 2015. Safety and immunogenicity of ricin vaccine, RVEc, in a phase 1 clinical trial. Vaccine 33:7299–7306. https://doi.org/10.1016/j.vaccine.2015.10.094.
39. Vitetta ES, Smallshaw JE, Coleman E, Jafri H, Foster C, Munford R, Schindler J. 2006. A pilot clinical trial of a recombinant ricin vaccine in normal humans. Proc Natl Acad Sci U S A 103:2268–2273. https://doi.org/10.1073/pnas.0510893103.
40. Vitetta ES, Smallshaw JE, Schindler J. 2012. Pilot phase IB clinical trial of an alhydrogel-adsorbed recombinant ricin vaccine. Clin Vaccine Immunol 19:1697–1699. https://doi.org/10.1128/CVI.00381-12.
41. Vance DJ, Mantis NJ. 2016. Progress and challenges associated with the development of ricin toxin subunit vaccines. Expert Rev Vaccines 15:1213–1222. https://doi.org/10.1586/14760584.2016.1168701.
42. Roy CJ, Brey RN, Mantis NJ, Mapes K, Pop IV, Pop LM, Ruback S, Killeen SZ, Doyle-Meyers L, Vinet-Oliphant HS, Didier PJ, Vitetta ES. 2015. Thermostable ricin vaccine protects rhesus macaques against aerosolized ricin: epitope-specific neutralizing antibodies correlate with protection. Proc Natl Acad Sci U S A 112:3782–3787. https://doi.org/10.1073/pnas.1502585112.
43. Castelletti D, Fracasso G, Righetti S, Tridente G, Schnell R, Engert A, Colombatti M. 2004. A dominant linear B-cell epitope of ricin A-chain is the target of a neutralizing antibody response in Hodgkin's lymphoma patients treated with an anti-CD25 immunotoxin. Clin Exp Immunol 136:365–372. https://doi.org/10.1111/j.1365-2249.2004.02442.x.
44. Vitetta ES, Stone M, Amlot P, Fay J, May R, Till M, Newman J, Clark P, Collins R, Cunningham D, Ghetie V, Uhr JW, Thorpe PE. 1991. Phase I immunotoxin trial in patients with B-cell lymphoma. Cancer Res 51:4052–4058.
45. Song K, Mize RR, Marrero L, Corti M, Kirk JM, Pincus SH. 2013. Antibody to ricin a chain hinders intracellular routing of toxin and protects cells even after toxin has been internalized. PLoS One 8:e62417. https://doi.org/10.1371/journal.pone.0062417.
46. Yermakova A, Klokk TI, Cole R, Sandvig K, Mantis NJ. 2014. Antibody-mediated inhibition of ricin toxin retrograde transport. mBio 5:e00995-13. https://doi.org/10.1128/mBio.00995-13.
47. Yermakova A, Klokk TI, O'Hara JM, Cole R, Sandvig K, Mantis NJ. 2016. Neutralizing monoclonal antibodies against disparate epitopes on ricin toxin's enzymatic subunit interfere with intracellular toxin transport. Sci Rep 6:22721. https://doi.org/10.1038/srep22721.
48. O'Hara JM, Mantis NJ. 2013. Neutralizing monoclonal antibodies against ricin's enzymatic subunit interfere with protein disulfide isomerase-mediated reduction of ricin holotoxin in vitro. J Immunol Methods 395:71–78. https://doi.org/10.1016/j.jim.2013.06.004.
49. Lemley PV, Amanatides P, Wright DC. 1994. Identification and characterization of a monoclonal antibody that neutralizes ricin toxicity in vitro and in vivo. Hybridoma 13:417–421. https://doi.org/10.1089/hyb.1994.13.417.
50. Turner KB, Hardy S, Liu JL, Zabetakis D, Lee PAB, Goldman ER, Anderson GP. 2017. Pairing alpaca and llama-derived single domain antibodies to enhance immunoassays for ricin. Antibodies 6:3. https://doi.org/10.3390/antib6010003.
51. Sebaugh JL. 2011. Guidelines for accurate EC50/IC50 estimation. Pharm Stat 10:128–134. https://doi.org/10.1002/pst.426.
52. Legler PM, Brey RN, Smallshaw JE, Vitetta ES, Millard CB. 2011. Structure of RiVax: a recombinant ricin vaccine. Acta Crystallogr D Biol Crystallogr 67:826–830. https://doi.org/10.1107/S0907444911026771.
53. Toth RT, IV, Angalakurthi SK, Van Slyke G, Vance DJ, Hickey JM, Joshi SB, Middaugh CR, Volkin DB, Weis DD, Mantis NJ. 2017. High-definition mapping of four spatially distinct neutralizing epitope clusters on RiVax, a candidate ricin toxin subunit vaccine. Clin Vaccine Immunol 24:e00237-17. https://doi.org/10.1128/CVI.00237-17.